Naoya Takahashi[1], Kelvin J. Richards[1], Niklas Schneider[1], H. Annamalai[1], Wei-Ching Hsu[1], and Masami Nonaka[2]

[1] International Pacific Research Center, School of Ocean and Earth Science and Technology, University of Hawai'i at Mānoa, Honolulu, Hawaii

[2] Japan Agency for Marine-Earth Science and Technology, Yokohama, Kanagawa, Japan

Corresponding author: Naoya Takahashi (naoyat@hawaii.edu)

Key Points:

- Formation mechanism of recent warm SST anomalies in the 2010s around Hawaii are investigated using the reanalysis products of ERA5 and ORAS5.
- These recent warm SST anomalies are mainly forced by anomalous downward latent heat flux, while oceanic meridional advection suppressed it.
- Both anomalies of latent heat flux and meridional advection are driven by the weakening of the zonal component of the surface.

Abstract

Warm sea surface temperature (SST) anomalies have been observed in the subtropical North Pacific around Hawaii in the recent decade, appearing from 2013. We examined the formation mechanisms of the warm SST anomalies in terms of relative contribution of atmospheric surface forcing and oceanic dynamics, using the latest reanalysis products from ECMWF (ERA5 for atmosphere and ORAS5 for ocean). Results of the mixed layer temperature budget diagnosis in the target area (10-20 ˚N and 180 ˚-160 ˚W) indicates that contributions from anomalous latent heat fluxes to the subtropical SST anomalies are dominant. Oceanic advective contributions are relatively small, dampen the SST anomalies, and are negatively correlated (r = –0.38) with the latent heat fluxes. For example, the +1.0K SST increased from 2011 to 2015 results from +1.5K contributions from sum of surface heat flux and –0.5K from meridional oceanic advection. The anti-correlation between atmospheric forcing and oceanic meridional advection reflects co-variations of wind-driven latent heat flux and meridional Ekman advection due to the weakening of the zonal component of the surface winds.

Plain Language Summary

Sea surface temperature (SST) is one of key factors controlling not only local but also global climate variabilities. SST around Hawaii has been higher than the usual state since 2013, and once reached 28.5 ˚C in 2015. SST anomaly also reached twice the standard deviation, indicating that this is a very rare case. In this study, we performed mixed layer temperature budget diagnostics using observational and reanalysis datasets to clarify which mechanism is responsible for the formation of the recent SST anomalies. The temperature

budget diagnostics revealed that the weakening of the latent heat release dominantly contributed to the formation of the warm SST anomalies, while oceanic horizontal advective process contributed to the damping of the anomalies. It is also found that the contributions from the two processes compensate each other. This can be explained by the physical connection between the latent heat release and meridional Ekman advection driven by trade wind changes.

1 Introduction

Although sea surface temperature (SST) anomalies (SSTAs) in the subtropical North Pacific have received less attention than the tropical SSTAs, they play an important role in modulating the climate variabilities around Hawaii (Chu, 1995; Chu & Chen, 2005; Luo et al., 2020; Ropelewski & Halpert, 1987; Taylor, 1984; Zhu & Li, 2017), as well as in the tropics and other remote regions and phenomena such as the El Niño/Southern Oscillation (ENSO) (M. A. Alexander et al., 2010; Amaya, 2019; Chang et al., 2007; Stuecker, 2018; Su et al., 2018; Vimont et al., 2001, 2003). In the 2010s, large positive SSTAs occupied most parts of the subtropical North Pacific. Figures 1a and 1b show snapshots of SSTAs during August 2015 and September 2018, respectively, normalized at each grid point by their standard deviation. In these months, the positive SSTAs around Hawaii region (green rectangles in Figs. 1a and 1b) reached twice the standard deviation. The spatial patterns of the anomalies were similar to the North Pacific Meridional Mode (NPMM; Chiang & Vimont, 2004), the dominant coupled SST-surface wind mode in the subtropical North Pacific. Figures 1 c and d show time-series of vertical mean temperature (T_m) and anomalies from its monthly climatology averaged vertically within the mixed layer and horizontally in the target region shown by the green rectangle in Figures 1 a and b. Two features of the recent SST and its anomaly around Hawaii stand out. First, absolute SST became higher than 28.5 $^\circ$C starting in 2015, leading to a record-breaking hot summer of 2015 in Hawaii (Zhu & Li, 2017). With SST exceeding the convective threshold (Graham & Barnett, 1987; Johnson & Xie, 2010; Sud et al., 1999; Zhang, 1993), slight changes in SST can alter atmospheric convection and likely impact the large-scale atmospheric circulation. Second, the positive SSTAs have been observed continuously since 2013 (Fig. 1d). While the standard deviation of the SSTAs in the subtropical North Pacific is less than 1 K, much smaller than that in the tropical Pacific, the normalized subtropical SSTAs reached twice the standard deviation. The abnormally warm SSTAs have not been recorded before 2010, indicating that this is a rare case.

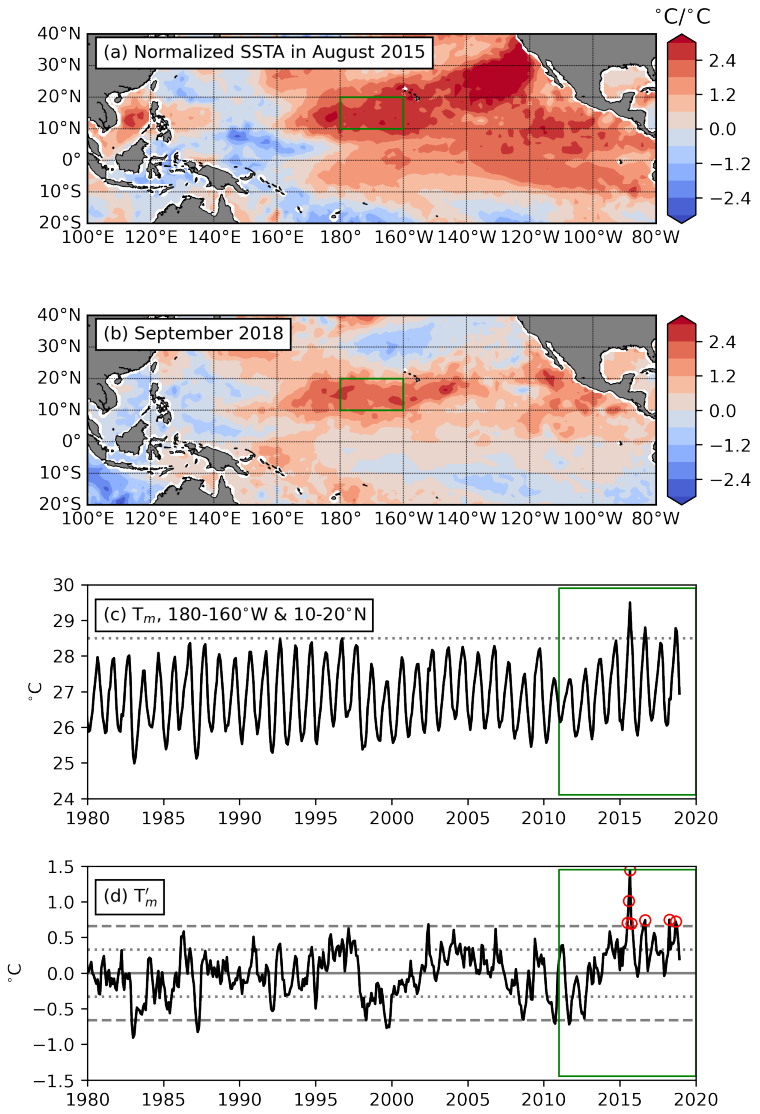

Figure 1. Snapshots of SSTAs divided by the standard deviation at each grid point in (a) August 2015 and (b) September 2018, obtained from ORAS5. Units are dimensionless. SSTAs are referenced to the January 1979 through December 2018 monthly climatology. Green rectangles in panels (a) and (b) represent the target region in the present study defined by 10-20 ˚ N, 180 ˚ -160 ˚ W. (c) Time series of domain averaged mixed layer temperature (T_m) in the target area, obtained from ORAS5. Definition of the mixed layer depth is given in section 2.2. Horizontal dotted line in panel (c) shows the 28.5C. (d) Same as (c), but for their anomalies from monthly climatology. Horizontal dotted and dashed lines in panel (d) indicate the ± 1 and 2 standard deviation of the anomalies

of T_m, respectively. Green rectangles in panels (c) and (d) represent the target period from 2011. Red circles in panel (d) represents the months with positive temperature anomalies that were larger than the twice the standard deviation.

Formation mechanisms of the subtropical SSTAs have been proposed by several previous studies (Chang et al., 2007; Chiang & Vimont, 2004; Vimont et al., 2001, 2003; Vimont & Kossin, 2007), including stochastic forcing by atmospheric variability, Seasonal Footprinting Mechanisms (e.g. Vimont et al., 2001), and oceanic dynamics associated with the trade wind changes variance (Alexander et al., 2006; Larson et al., 2018; Anderson et al., 2013; Anderson & Perez, 2015). Seasonal Footprinting is a mechanism whereby wintertime atmospheric variability in the mid-latitudes provides a "footprint" of SST to the ocean through changes in the net surface heat flux, and the SST footprint persists into the summertime and affects the atmospheric circulation anomalies in the subtropical regions in the following wintertime. Although the proposed mechanism has a timescale of seasonal to about one year, the recent warm SSTAs have continued on inter-annual or decadal timescales (Fig. 1d). Thus, the recent inter-annual SSTAs could be different from the known mechanism. For decadal SST anomalies associated with the NPMM, previous studies pointed out the key role of the stochastic forcing of the southern lobe of the North Pacific Oscillation (Di Lorenzo et al., 2015) or teleconnections influence from Atlantic Multi-decadal Oscillation to the subtropical high (J.-Y. Yu et al., 2015). As described above, the controlling factors for the subtropical SSTAs is basically recognized as the surface heat flux anomalies. However, recent studies have shown the importance of other processes in controlling the subtropical SSTAs using numerical simulations. For example, Ekman transport by trade wind stress can decreases the subtropical SST variance (Alexander et al., 2006; Larson et al., 2018). Regarding the influence of NPMM on the ENSO (i.e. impact of extra tropics on the tropics), the 'Trade Wind Charging' of equatorial subsurface heat content by surface wind stress curl anomalies related with the NPMM are also pointed out (Anderson et al., 2013; Anderson & Perez, 2015). The role of oceanic dynamics in the mechanism of the SSTA evolution in the subtropical North Pacific is still unclear, particulary for the relative importance of the atmospheric and oceanic processes for the subtropical SSTAs on inter-annual timescales.

One of prominent events which may affect the recent subtropical SSTAs is the marine heat wave, which brings warm water from the western North Pacific to the eastern North Pacific and affects the subtropical SSTAs (Amaya et al., 2020; Bond et al., 2015; Scannell et al., 2020). Several previous studies have investigated the characteristics of the recent marine heat waves in 2010s in the northeastern Pacific, called Blob in 2014 (Bond et al., 2015) and Blob 2.0 in 2019 (Amaya et al., 2020), and their impacts on the subsurface temperature anomalies in the subtropical North Pacific through advective processes. Scannell et al. (2020) investigated differences in stratification between the two events, suggesting that warm water near-surface anomalies penetrated into the deeper layer because of the weaker stratification in 2014 compared with that in 2019. Mixed layer depth plays a key role in modulating the sensitivity of mixed layer

temperature to the surface heat flux, in addition to the horizontal transport of water with temperature anomaly. Recent studies revealed that upper ocean warming response to future climate change is expected to shoal the mixed layer (M. A. Alexander et al., 2018; Amaya et al., 2021; Capotondi et al., 2015). However, the importance of mixed layer depth for inter-annual and decadal SSTAs is not well understood. Thus, further investigations are needed of the formation and maintenance of the recent abnormally warm subtropical SSTAs on longer timescales than the inter-annual. We focused on the recent continuous warm SSTAs around Hawaii, investigated their formation mechanism based on the mixed layer temperature budget equation, and addressed the following three questions. (1) What are the relative contributions of the atmospheric and oceanic processes to the recent positive SSTAs? (2) What physical processes are responsible for each anomalous contribution? (3) Is there any relationship between the atmospheric and oceanic processes?

The remainder of this paper is organized as follows. Section 2 introduces the reanalysis products and the mixed layer temperature budget used to investigate the mechanism of the inter-annual SST. Section 3 describes characteristics of recent warm SSTAs in 2010s and related variability of subsurface temperature in the subtropical North Pacific. Section 4 discusses the formation mechanism of the recent SSTAs based on mixed layer temperature budget analysis. We quantified the relative contribution of atmospheric and oceanic processes to the SSTA formation and examined the relationship between the two processes. Section 5 summarizes and discusses findings.

2 Datasets and Methods

2.1 Reanalysis products

To obtain monthly-mean states of the atmosphere and ocean in the subtropical North Pacific, we used the latest reanalysis products provided by European Centre for Medium-Range Weather Forecasts (ECMWF) from January 1979 to December 2018. The fifth generation atmospheric reanalysis from ECMWF (ERA5; Hersbach et al., 2020) supplied shortwave radiation (SW), longwave radiation (LW), sensible heat flux (SH), latent heat flux (LH), surface wind speed (ws_{10}), specific humidity (q), and sea level pressure (SLP). This dataset has a horizontal resolution of 0.25° and 137 vertical levels whose resolution is finer than that of ERA-Interim. The Ocean Reanalysis System 5 (ORAS5; Zuo et al. 2018) reanalysis product is utilized to estimate the oceanic properties. This dataset has a horizontal resolution of 1° and 75 vertical levels with a 1 m resolution near the surface, including 24 levels in the upper 100 m. ORAS5 uses three-dimensional variational method with a 5-day assimilation cycle. The reanalysis assimilates observations of SST and subsurface temperature and salinity profiles. We obtained water temperature (T), zonal velocity (u), meridional velocity (v), wind stress, and sea surface height from ORAS5 datasets. Finally, we calculated the mixed layer temperature budget terms shown in next subsection. The anomalies of each variable are estimated as the difference from the 1979-2018 averaged seasonal cycle.

To check the accuracy of the products and the dependency of the results on the products, the domain averaged time-series of surface heat fluxes of ERA5 in the target region are compared with other reanalysis products (ERA-Interim; Dee et al., 2011, NCEP-CFSRv2; Saha et al., 2014) and observational datasets (J-OFURO3; Tomita et al., 2019, CERES; Kato et al., 2018, OAFlux; Yu et al., 2008). Similar comparisons were conducted for oceanic properties in the mixed layer from ORAS5 with SODA3 (Jackett et al., 2006) and ECCOv4r4 (Fukumori et al., 2019). Results of the comparisons are shown in Figures 2 and 3, and suggest that anomalies of surface heat fluxes, oceanic temperature, and oceanic currents are consistent across the various datasets. Note that our results thus are insensitive to the choice of both atmospheric and oceanic datasets.

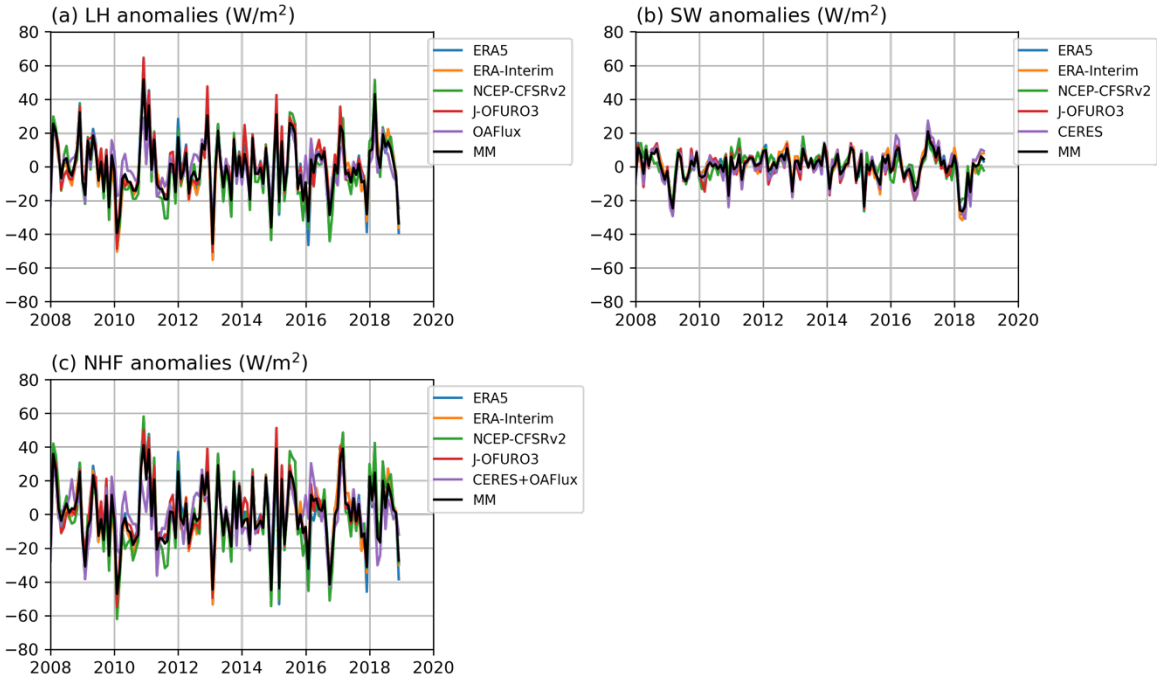

Figure 2. Comparison of the time series of domain averaged anomalies of surface heat flux components in the target area (10-20 ° N and 180 ° -160 ° W); (a) shortwave radiation (SW; W/m^2), (b) latent heat flux (LH; W/m^2), and (c) net surface heat flux (NHF; W/m^2). Downward heat fluxes are defined as positive. Colors show the result obtained from different sources. Reanalysis products; ERA5, ERA-Interim, NCEP-CFSRv2. Satellite-based observation; CERES, OAFlux, J-OFURO3 . MM : multi-product mean value calculated from the three reanalysis products from 1982 to 2018.

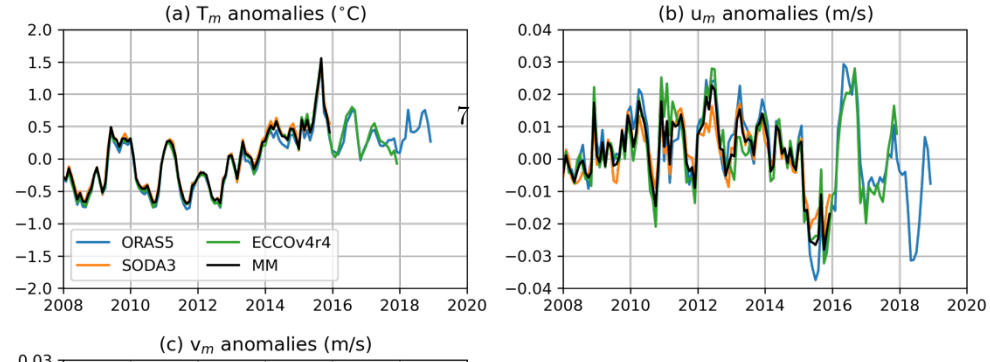

To reveal the formation mechanism of the warm SST anomalies from 2013 to the present, an analysis of the mixed layer temperature budget was conducted. Following Moisan and Niiler (1998), we write the mixed layer temperature budget equation as

$$\frac{\partial \{T_m\}}{\partial t} = \underbrace{\left\{\frac{Q}{\rho c_p H}\right\}}_{A} \underbrace{-\left\{\frac{\partial}{\partial x} u_m (T_m - T_r)\right\}}_{B} \underbrace{-\left\{\frac{\partial}{\partial y} v_m (T_m - T_r)\right\}}_{C} \underbrace{-\left\{\frac{(T_m - T_r)}{H} \mathbf{u_m} \bullet H\right\}}_{D_1} \underbrace{- \left\{\frac{(T_m - T_{-H})}{H} \frac{\partial H}{\partial t} + \frac{(T_r - T_{-H})}{H} (\mathbf{u_{-H}} \bullet H + w_{-H}) + \frac{1}{H} \bullet \left(\int_{-H}^{0} \widehat{\mathbf{u}}\right.\right.}_{D_2}$$

where T is temperature, Q is net surface heat flux, ρ is the density of the water, c_p is the specific heat, H is mixed layer depth (MLD), $\mathbf{u}$ is the horizontal component of the velocity vector, and w the vertical component. MLD is defined as the layer whose density increases by 0.064 kg/m^3 from that at 5m. The density increase corresponds to a temperature decrease of 0.2 $^\circ$C with a specific surface condition; salinity is 35 psu and temperature is 27 $^\circ$C at 5 m. Subscript m represents the vertically averaged variable in the mixed layer; $X_m = \frac{1}{H}\int_{-H}^{0} \mathrm{X}\ \mathrm{dz}$, and subscript $-H$ represents the values at the bottom of the mixed layer. We considered temperature anomalies averaged in the large target box from 10-20N and 180-160W, and calculated volume averaged budget terms over a large horizontal domain, as in $\{X\} = \frac{1}{V_D}\iiint_D \mathrm{X}\ \mathrm{dx}\ \mathrm{dy}\ \mathrm{dz}$, where V_D is the total volume of the domain. Advection in the equation is expressed in flux form with the volume averaged reference temperature (T_r), as in $T_r \equiv \{T_m\}$ (Lee et al., 2004; Soares et al., 2019) .The flux form removes spatial averaged local avective processes that redistribute heat within the domain, therefore, it exactly captures external heat source and sink that control the spatially averaged temperature. For calculations of the net surface heat flux (Q), we subtract the penetration of the shortwave radiation across the bottom of the mixed layer from the net surface heat flux at the sea surface.

Term A on the right-hand side (RHS) represents the surface forcing, terms B and C represent the oceanic dynamics with lateral advection, respectively. Terms D represents the vertical advection, subsurface processes (entrainment and lateral induction), and the divergence of the horizontal heat fluxes ($\widehat{X}$) that differ from the vertical mean. We calculated the left-hand side (LHS) term and five RHS terms from A to D2, and residual (R) is obtained as the difference between the LHS term and sum of the five terms in the RHS. The residual includes unresolved process not explicitly shown in Equation 1, such as diffusive processes, differences in atmospheric forcing (ORAS5 is forced with ERA-Interim) and possible heat sources from the oceanic assimilation. The latter is potentially problematic, although in the case considered here it does not overly compromise our conclusions.

3 Oceanic temperature anomalies in 2010s around Hawaii

To summarize the characteristics of the abnormally warm SSTAs, in 2010s around Hawaii including subsurface temperature and mixed layer depth, we plotted the time-depth cross sections of oceanic temperature anomaly and the

domain averaged MLD obtained from ORAS5 (Figure 4). Consistent with the appearance of the warm SSTAs (Figure 1), warm water anomalies appeared within the mixed layer since 2013. Cold water anomalies appear under the warm surface water anomalies except from 2016 to 2018, indicating that the temperature variability above and below the mixed layer is not closely linked. In addition, time-series of the vertical mean temperature in the mixed layer are almost the same as that of SST (Figure 1). This suggests that SSTAs in the target region are controlled by surface forcing or ocean dynamics within the mixed layer, rather than by vertical intrusions from deeper layers. Our investigation based on the mixed layer temperature budget analysis, therefore, is well suited to identify the relative contribution of atmospheric and oceanic processes to the recent SSTAs. Warm water anomalies at depth from 2016 to 2018 are potentially related to the warm water propagation from northeastern Pacific to around Hawaii.

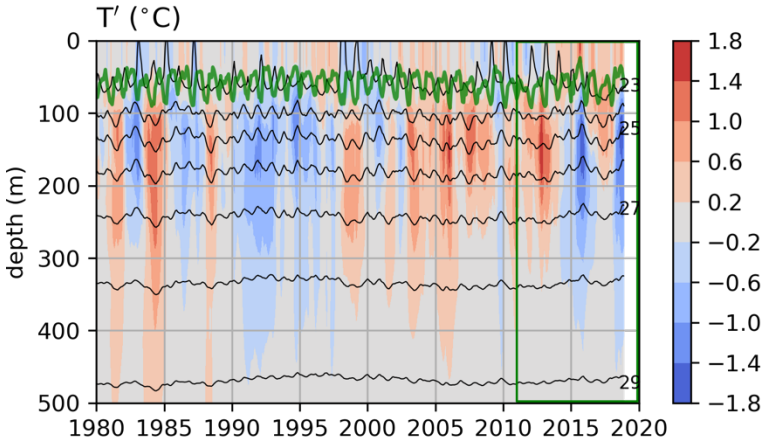

Figure 4. Time-depth cross section of oceanic temperature anomalies (shade; Unit is ˚C) in the target region obtained from ORAS5. Black contours represent isopycnal surface (contour; Unit is kg/m^3; counter Interval is 1 kg/m^3.) Green line represents the domain averaged mixed layer depth.

4 Mixed layer temperature budget diagnosis

4.1 Results of mixed layer temperature budget

In this section, we determine the dominant factors in the formation and maintenance of the warm SSTAs around Hawaii from 2011 to 2019 using the mixed layer temperature budget equation (Eq. 1). Figure 5a and 5b show the time-series of each term in the budget equation and its anomaly, respectively. Anomalous budget terms are smoothed by a 13-month running average to focus on a inter-annual variability. The time-series of the heat budget terms show clear seasonality (Fig. 5a), and seasonal variations of the total tendency of T_m are mostly explained by the term associated with the surface forcing (term A). The anomalous budget in the recent decade suggests that warming tendency are

attributed to the surface forcing from 2011 to 2014 and from 2017 to 2018 (Fig. 5b). To further investigate the accumulation impact of the anomalous heat budget terms on the recent positive SSTAs, we time integrate the terms from January 2011 (Fig. 5c). The results indicate that the accumulation of the anomalous surface forcing (term A) explains the phase of positive SSTAs in 2010s, but overestimates its magnitude. Anomalous meridional advection (term C) reduces the SST anomalies such that the increase of SST by 1.0 ˚C from 2011 to 2015 is explained by a 1.5 ˚C increase due to the surface heat flux and a 0.5 ˚C decrease by the meridional advection (Fig. 5c). Contributions from zonal advection (term B) are relatively small compared to terms A and C, but contribute to the gradual increase of SSTAs from 2011 to 2016 by 0.2 ˚C. Vertical processes and residual (terms D and R) are negligible compared to surface forcing and horizontal advection. In the next subsections, we investigate the details of each term and physical background behind the recent anomalous budget terms.

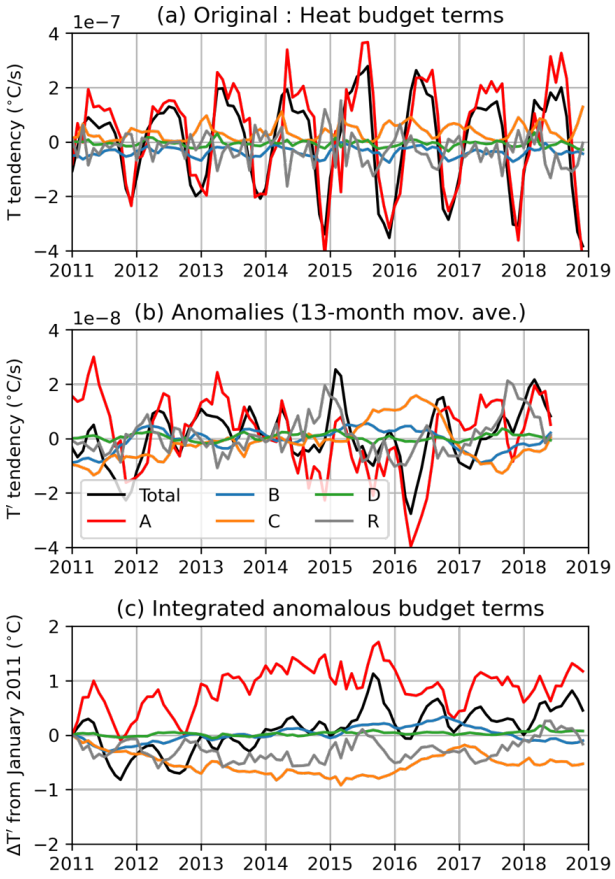

Figure 5. Time-series of domain averaged (a) total mixed layer temperature budget terms (Unit is ˚C/s), (b) anomalous budget terms relative to the

monthly climatology from 1979 to 2018 and smoothed with a 13-month moving average (Unit is $^\circ$C/s), and (c) integrated anomalous budget terms from January 2011 (Unit is $^\circ$C). Black, red, blue, orange, green, and grey lines represent budget term derived from all processes (Total), surface forcing (A), zonal advection (B), meridional advection (C), vertical oceanic process (D), and unresolved process or dataset error (R), respectively.

4.2 Atmospheric components

First, we investigated the components of anomalous positive surface heat flux anomaly from 2011 to 2019. Figure 6a decomposes the anomalous surface heat flux into its SW, LW, SH, and LH component from 2011, where positive values correspond to downward heat fluxes. The results show that most of the anomalous positive net heat surface fluxes were determined by the anomalous LH except for the period after 2017. During the periods from 2011 to 2014, SW anomalies were as positive as LH anomalies. However, LW anomalies are negative during the same, offsetting the SW anomalies. Positive LH anomalies dominate in early 2010s. A decomposition of the LH anomalies was conducted to examine the controlling factors, i.e. surface wind speed and humidity, via

$$\mathrm{LH}^{'} = \rho_a L C_E \left[\mathrm{ws}_{10}^{'} \left(\overline{q_s} - \overline{q_a} \right) + \overline{\mathrm{ws}_{10}} \left(q_s^{'} - q_a^{'} \right) + \mathrm{ws}_{10}^{'} \left(q_s^{'} - q_a^{'} \right) \right], \tag{2}$$

where ρ_a is the atmospheric density, L is the latent heat of vaporization, C_E is the bulk coefficient, q_s is specific humidity at the sea surface, q_a is specific humidity near the sea surface. The overbar denotes the climatological mean for each month and prime denotes the anomaly from the mean. Figure 6b shows the three LH components on the RHS of Equation 2 due to anomalous surface wind speed (ws_{10}'), difference of saturation humidity at the sea surface and humidity at a height of 10 m (q'), and non-linear effect (ws_{10}'q'). From late 2011 to 2012, the wind-driven LH anomalies were negative due to the anomalous strong wind speed while the moisture-driven part was positive due to the negative SSTAs. However, during 2013 to 2015 both terms reverse signs. Dominant component for the positive LH anomalies changes during the period. Weak surface wind speed anomalies are likely to be a key factor to generate the recent positive SSTAs, particularly from 2013. As seen in Figure 2, the LW and SW components, as well as the net heat flux, computed from different reanalysis products are very similar.

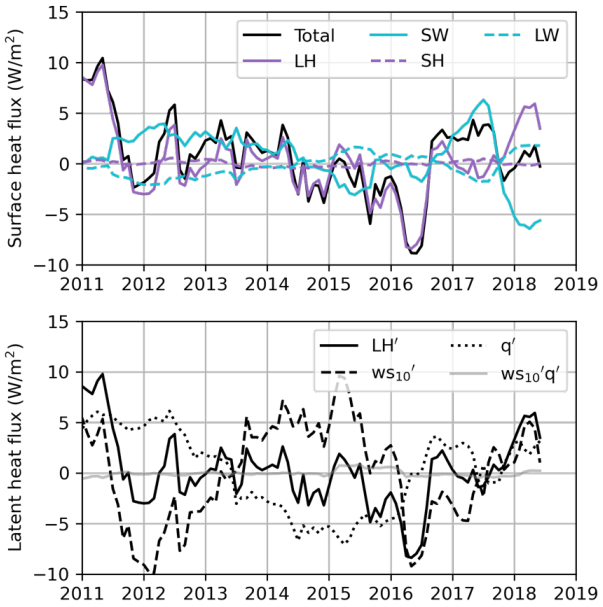

Figure 6. Time-series of domain averaged (a) anomalous surface heat flux components, NHF; net heat flux, SW; shortwave radiation, LW; longwave radiation, SH; sensible heat flux, LH; latent heat flux. (b) Time-series of decomposed LH anomalies, q ; LH anomalies derived from moisture anomaly, ws_{10} ; LH anomalies derived from surface wind speed anomaly, ws_{10} q ; LH anomalies derived from nonlinear effect of moisture and surface wind speed anomalies. All time-series are averaged by 13-month moving windows.

Figure 7a shows the time series of domain averaged SST and ws_{10} anomalies. These time series are negatively correlated (r= –0.48, 99% significance), indicating the surface wind speed has weakened in the target region when the warm SSTAs appeared, and consistent with the suppression of the wind-driven LH release as a dominant factor for the positive SSTAs. To investigate the atmospheric circulation field that modulated the ws_{10} anomaly in the target region, we regress SLP and surface winds with the domain averaged ws_{10} (Fig. 7b). Regression ceofficients show a north-south dipole pattern of SLP anomalies, very similar to the North Pacific Oscillation (NPO) pattern (e.g. Kutzbach, 1970; Rogers, 1981),. The southern lobe of SLP regression dipole, located around 30 ˚ N and 180 ˚ , increases the surface wind speed around Hawaii. Note that the SLP anomalies shown in Figure 7b correspond to a strong surface wind speed in the target region. Therefore, the continuous negative ws_{10} anomaly associated with the low SLP anomalies in the mid-latitude is considered to be an important factor for the suppression of the LH release in the recent decade.

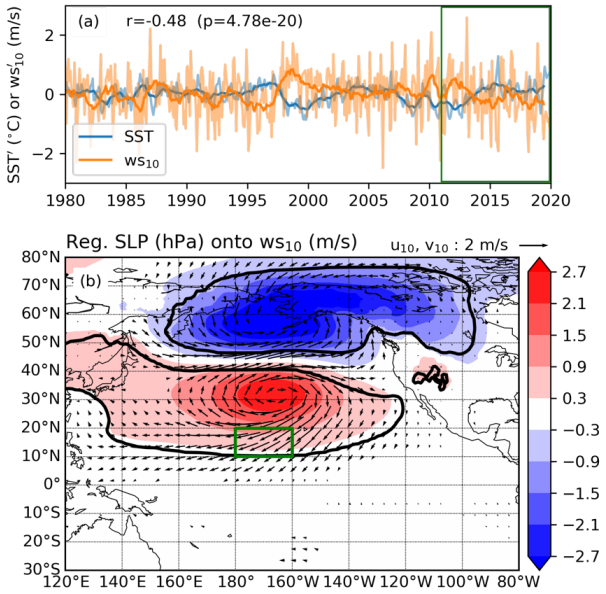

Figure 7. (a) Time-series of domain averaged SST (blue) and ws_{10} (orange) anomalies in the target region. Thin and thick lines represent original anomalies and moving averaged anomalies with 13-month windows, respectively. Numbers at top left corner indicates the correlation coefficient between SST and ws_{10} anomalies (r) and p-value. (b) Regression coefficients of the moving averaged anomalies of sea level pressure (SLP; shade; Unit is hPa) and surface horizontal wind (u_{10} and v_{10}; Unit is m/s) with domain averaged ws_{10} from 1979 to 2019. Black lines indicate the area with the SLP anomalies with 95% significance.

4.3 Oceanic components

4.3.1 Oceanic lateral advection

Next, we investigated the reason why oceanic meridional advection suppresses and zonal advection amplifies the positive SSTAs from 2013 to the present. Here we are using the flow field from the ORAS5 reanalysis. As shown in Figure 3, very similar anomalies, in terms of amplitude and phase, in the mixed-layer averaged eastward and northward velocity components are found in other reanalyses.

In Figure 8, horizontal advection anomalies are decomposed into geostrophic, wind-driven Ekman, and residual components

$$U = \underset{U_g}{-\frac{g}{f}\frac{\partial h}{\partial y}} + \underset{U_e}{\frac{\tau_y}{\rho H}} + U_r, \tag{3}$$

$$V = \underset{V_g}{\frac{g}{f}\frac{\partial h}{\partial x}} - \underset{V_e}{\frac{\tau_x}{\rho H}} + V_r, \tag{4}$$

where f is the Coriolis parameter, g is the gravitational acceleration, h is sea surface height, and τ is wind stress. First, second, and third terms on the RHS are geostrophic (U_g, V_g), Ekman (U_e, V_e), and residual (U_r, V_r) components of each horizontal velocity (Fig. 8). The residual is negligible. Climatological oceanic currents in the target region are north-westward (not shown), so that relatively warm and cold waters are transported from the tropics and eastern North Pacific into the target region. Climatological meridional advection carries warm waters northward, so that weakened meridional currents or meridional temperature gradients dampen the positive SSTAs. Decomposing the Ekman meridional advection anomalies into current-driven or temperature gradient-driven components suggests that a weakening of both meridional current and temperature gradients are important in suppressing the recent positive SSTAs (not shown). Similar analysis were conducted for the geostrophic components of the anomalous zonal advection, and suggest that a reduction of the zonal current contributes to the increasing SST, while changes of the temperature gradient are small (not shown). Since meridional advection contributes a larger share to recent SSTAs changes than the zonal advection (Fig. 5c), the Ekman meridional advection process driven by anomalous zonal wind stress is dominant.

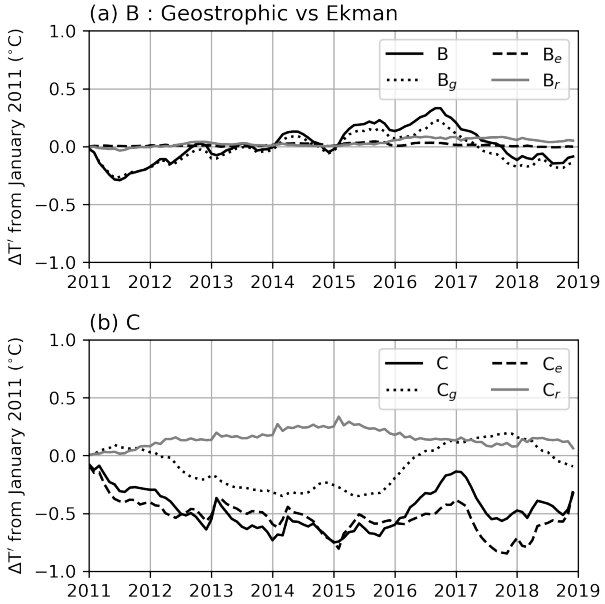

Figure 8. Same as Figure 5c, but for decomposed anomalies of (a) zonal advection and (b) meridional advection derived from geostrophic (B_g and C_g), Ekman (B_e and C_e), and residual components (B_r and C_r).

We further investigate the relationship between surface wind speed and the components of the oceanic advection (i.e. geostrophic, Ekman, and residual components). Figure 9 shows maps of the regression coefficients of oceanic horizontal advection (i.e. term B + term C in Equation 1) and of horizontal

current anomalies onto the domain averaged ws_{10} anomaly in the target area. Significant anomalies of warm advection with north-westward currents appear in the southern part of the target region where the surface wind speed is strong (Fig. 9a). The result indicates that the regression coefficient of the advection is dominated by the Ekman component and not the geostrophic and residual components. It also suggests that the Ekman component of the warm water advection from the tropics is enhanced by the strengthening of the surface wind, especially by the zonal component. It consistent with the meridional component of Ekman advection being enhanced by the zonal wind stress. Thus, the negative ws_{10} anomaly, particulary from 2011, is also associated with a weakening of the meridional Ekman transport of warm water from the tropics, resulting in the suppression of the positive SSTAs.

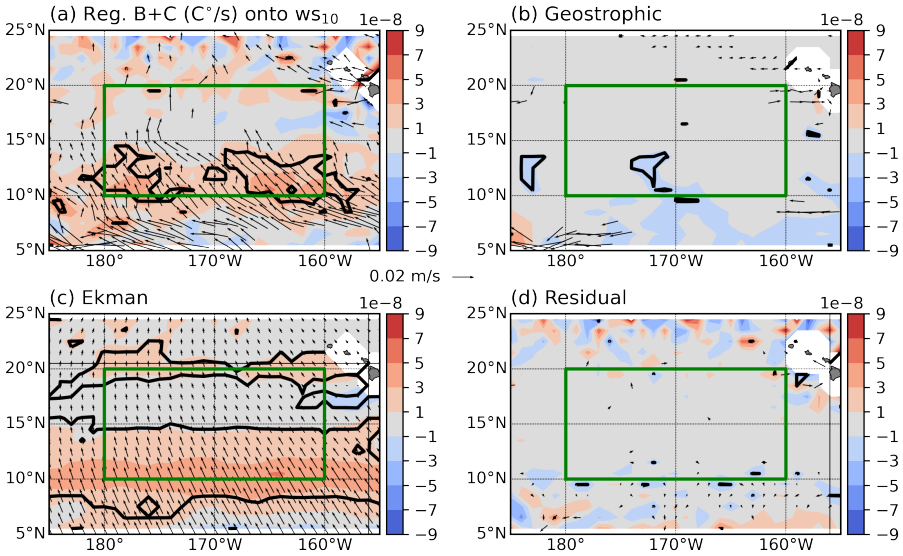

Figure 9. Same as Figure 7, but for anomalous heat budget term derived from oceanic horizontal advection (B+C; Unit is ˚C/s) and oceanic horizontal currents in the mixed layer(u_m and v_m; Unit is m/s). (a) Total oceanic advection, (b) Geostrophic component, (c) Ekman component, and (d) residual component.

4.3.2 Mixed layer depth

Our results pointed out that the main reason for the recent positive SSTAs was anomalous heat budget term related with the surface forcing (Fig. 5c), however, the term is derived from the anomalies of not only surface heat flux but also MLD. Therefore, we further investigated the impact of the MLD anomalies on the recent SSTAs using the equation below.

$$\left\{\frac{Q}{\rho c_p H}\right\}' \sim \left\{\frac{Q'}{\rho c_p \overline{H}}\right\} - \left\{\frac{\overline{Q}H'}{\rho c_p \overline{H}^2}\right\} - \left\{\frac{Q'H'}{\rho c_p \overline{H}^2}\right\}, \tag{5}$$

where the overbar denotes the climatological monthly mean and prime denotes the anomaly from the mean. Figure 10a shows time series of domain averaged MLD anomaly in the target region from 2011. MLD anomalies were positive in the early 2010s, then negative from 2013 to 2015, and positive again from 2016. Generally, positive MLD anomalies suppress the SST variability; e.g. climatological heating in summer and cooling winter are suppressed. Figure 10b shows the time-series of the integration of anomalous term A from January 2011, but for decomposed anomalies derived from anomalous surface heat flux (Q'), anomalous MLD (H'), and combined impact of those anomalies (Q'H'). The result indicates that positive SSTAs by surface forcing (i.e. term A) can be explained by surface heat flux anomalies (Fig. 10b). In contrast, contribution from MLD anomalies worked to suppress the positive SSTAs due to the thick MLD anomalies from 2011 to 2012. While contribution from MLD anomalies was not key for the positive SSTAs in 2010s, it significantly contributed to the dramatically increasing SST by about +1 ˚ C from June to September in 2015 (orange line in Fig. 10b).

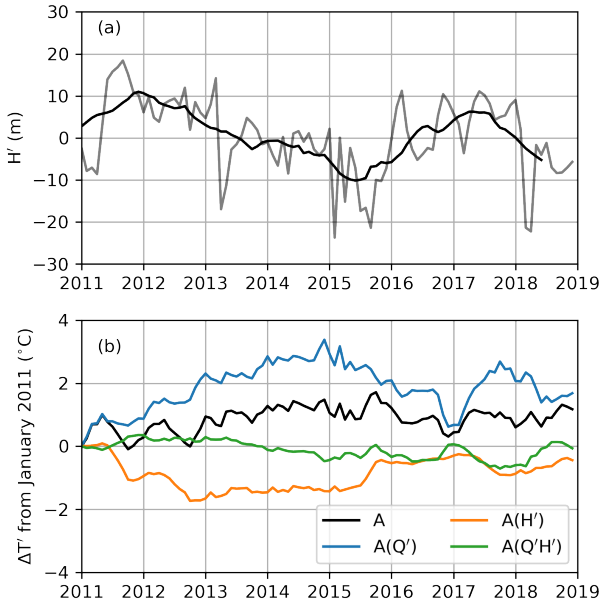

Figure 10. (a) Time-series of domain averaged mixed layer depth (MLD) anomaly in the target region. Thin and thick lines represent original and 13-month moving averaged time-series, respectively. (b) Same as Figure 5c, but for decomposed anomalies of surface forcing derived from surface heat flux

anomaly (Q'), MLD anomaly (H') and combined effect (Q'H').

4.4 Relationship between atmospheric and oceanic components

In the previous subsections, we found that the suppression of the LH release and meridional warm water transport from the tropics played a key role in modulating the recent SSTAs around Hawaii. Finally, we examined the relationship between anomalous surface forcing and oceanic advection processes. Figure 11 shows the lag correlation coefficients between the domain averaged terms of surface heat flux (A) and the oceanic advections (B/C). The correlation coefficients at zero lag between terms A and C or the sum of B and C are -0.38 and -0.31, respectively, and are both statistically significant at 95%. Correlation coefficients between terms A and B at zero lag are insignificant. While the correlation coefficients at small lag are modest, significant positive correlations appear between lags of -18 and -10 months in all of advection terms. The negative zero lag correlations between terms A and C suggest the contributions from surfacing forcing and meridional advection significantly co-vary and compensate for each other. Additional lag correlation analysis between anomalies of the surface wind speed and each heat budget terms also shows the significant correlation coefficients at zero lag; r= -0.72 between ws_{10} and term A, +0.55 between ws_{10} and term C (not shown). Therefore, the co-variations of surface forcing and oceanic meridional advection are driven by the surface winds, particularly for zonal component.

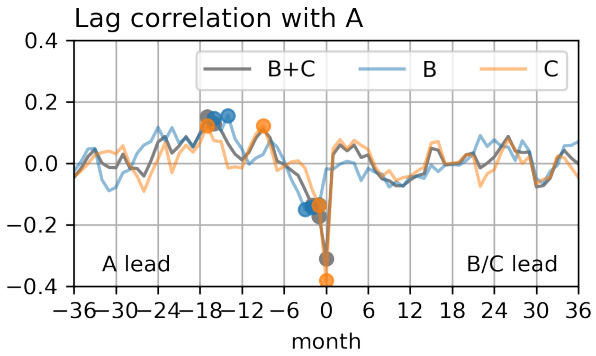

Figure 11 Lag correlation coefficient between A and sum of B and C (black), between A and B (blue), and between A and C (orange) derived from unfiltered anomalies from 1979 to 2019 in the target region. Circles indicate where the coefficient at a certain lag month exceeds the 95% significance level.

5 Summary and Discussion

This study explores the formation mechanism of the warm SST anomalies around Hawaii in a recent decade based on mixed layer temperature budget equation using the latest atmospheric and oceanic reanalysis products (here we use ERA5 and ORAS5, but show the results are not overly sensitive to the reanalysis products used). The SST increase from January 2011 to December

2015 results from anomalous positive wind-driven anomalies of LH flux. The wind-driven LH releases in the target region were suppressed by a reduction of the surface wind speed due to the spatial pattern of SLP anomalies associated with the North Pacific Oscillation. Oceanic meridional advection made a relatively small, but important, contribution in acting to suppress the warm SST anomalies. The mechanisms responsible for the anomalous negative meridional advection were the suppression of the meridional Ekman transport of warm water from the tropics driven by the anomalous zonal components of the surface wind speed. Further lag correlation analysis among the heat budget terms suggests that the contributions of surface heat flux and meridional advection to the SSTAs are negatively correlated with statistical significance. In addition, the results implied that the contributions from atmospheric and oceanic processes to the SSTAs in subtropical North Pacific compensate each other.

Investigation of the impact of the MLD anomalies on the positive SSTAs from 2013 to the present showed that its contribution is minor (Fig. 10b). However, the MLD anomalies significantly contributed to the dramatically increasing SST by about $+1\,^{\circ}$C within a short term, for example from June to September in 2015. It suggests that MLD anomalies were not a dominant factor in modulating the SSTAs on inter-annual or decadal timescales, but are dominant on short timescales, such as the event associated with the rapid increasing SST. Amaya et al. (2020) investigated the role of MLD anomalies for the abnormally warm SST anomalies associated with the Blob 2.0 in northeastern Pacific based on oceanic reanalysis products, suggesting that the anomalous thin MLD is one of important drivers. This result is consistent with the importance of the anomalous MLD contribution to the rapid increasing SSTAs in the subtropical North Pacific in the summer of 2015, as we have shown. While our results did not show a significant contribution of MLD anomalies to the inter-annual SSTAs, the role of MLD anomalies for SSTAs variability on not only short but also long timescales is still worth further investigation based on the model outputs or using long-term observational records that can capture the trends.

Finally, we consider the physical background controlling the surface wind speed anomalies around Hawaii. We have concluded that SLP anomalies associated with the NPO pattern play a key role to induce the surface wind speed anomalies around Hawaii on inter-annual or decadal timescales. On seasonal or shorter timescales a north–south seesaw pattern of SLP anomalies over the North Pacific has been identified (Kutzbach, 1970; Linkin & Nigam, 2008; Rogers, 1981). Similar patterns of SLP anomalies related with the NPO pattern have been also be found on decadal timescales by several previous studies (Furtado et al., 2012; Di Lorenzo et al., 2010, 2015), closely linked with the Central Pacific ENSO (Ashok et al., 2007; Kao & Yu, 2009; Kug et al., 2009; Ren & Jin, 2011) or North Pacific Gyre Oscillation (Di Lorenzo et al., 2008). To further our understanding of the mechanism of the surface wind speed variabilities in the subtropical North Pacific on inter-annual or decadal timescales, the linkage with tropical climate variability on such a longer timescale should be further

investigated (Amaya, 2019; Furtado et al., 2012; Di Lorenzo et al., 2010, 2015; Sanchez et al., 2019; Stuecker, 2018), as well as the teleconnection influences from other ocean basins (Lim et al., 2019; Yu et al., 2015).

Acknowledgments, Samples, and Data

This research was supported by the Japan Agency for Marine-Earth Science and Technology through JAMSTEC IPRC Collaborative Research (JICore). Data were provided by Asia-Pacific Data Research Center; http://apdrc.soest.hawaii.edu/, which is a part of the International Pacific Research Center at the University of Hawai i at Mānoa, funded in part by the National Oceanic and Atmospheric Administration (NOAA). Data sources of reanalysis products are listed below; ERA5 from https://cds.climate.copernicus.eu/cdsapp#!/dataset/reanalysis-era5-single-levels-monthly-means, ERA-Interim from http://apps.ecmwf.int/datasets/, NCEP-CFSv2 from http://cfs.ncep.noaa.gov/pub/raid1/cfsv2/reforecast.monthly.time/, ORAS5 from https://www.cen.uni-hamburg.de/en/icdc/data/ocean/easy-init-ocean/ecmwf-oras5.html, SODA3 from https://www2.atmos.umd.edu/~ocean/, and ECCOv4r4 from https://www.ecco-group.org/products-ECCO-V4r4.htm. J-OFURO3 products are downloaded from https://j-ofuro.isee.nagoya-u.ac.jp/en/. CERES data were obtained from the NASA Langley Research Center CERES ordering tool at http://ceres.larc.nasa.gov/. The global ocean heat flux and evaporation data provided by the Woods Hole Oceanographic Institution OAFlux project (http://oaflux.whoi.edu) were funded by the NOAA Climate Observations and Monitoring (COM) program.

References

Alexander, M., Yin, J., Branstator, G., Capotondi, A., Cassou, C., Cullather, R., et al. (2006). Extratropical Atmosphere–Ocean Variability in CCSM3. *Journal of Climate*, *19*(11), 2496–2525. https://doi.org/10.1175/JCLI3743.1Alexander, M. A., Vimont, D. J., Chang, P., & Scott, J. D. (2010). The Impact of Extratropical Atmospheric Variability on ENSO: Testing the Seasonal Footprinting Mechanism Using Coupled Model Experiments. *Journal of Climate*, *23*(11), 2885–2901. https://doi.org/10.1175/2010JCLI3205.1Alexander, M. A., Scott, J. D., Friedland, K. D., Mills, K. E., Nye, J. A., Pershing, A. J., & Thomas, A. C. (2018). Projected sea surface temperatures over the 21st century: Changes in the mean, variability and extremes for large marine ecosystem regions of Northern Oceans. *Elementa: Science of the Anthropocene*, *6*. https://doi.org/10.1525/elementa.191Amaya, D. J. (2019). The Pacific Meridional Mode and ENSO: a Review. *Current Climate Change Reports*, *5*(4), 296–307. https://doi.org/10.1007/s40641-019-00142-xAmaya, D. J., Miller, A. J., Xie, S.-P., & Kosaka, Y. (2020). Physical drivers of the summer 2019 North Pacific marine heatwave. *Nature Communications*, *11*(1), 1903. https://doi.org/10.1038/s41467-020-15820-wAmaya, D. J., Alexander, M. A., Capotondi, A., Deser, C., Karnauskas, K. B., Miller, A. J., & Mantua, N. J. (2021). Are Long-Term Changes in Mixed Layer Depth Influencing North Pacific Marine Heatwaves? *Bulletin of the American Meteorological Society*,

102(1), S59–S66. https://doi.org/10.1175/BAMS-D-20-0144.1Anderson, B. T., & Perez, R. C. (2015). ENSO and non-ENSO induced charging and discharging of the equatorial Pacific. *Climate Dynamics*, *45*(9–10), 2309–2327. https://doi.org/10.1007/s00382-015-2472-xAnderson, B. T., Perez, R. C., & Karspeck, A. (2013). Triggering of El Niño onset through trade wind-induced charging of the equatorial Pacific. *Geophysical Research Letters*, *40*(6), 1212–1216. https://doi.org/10.1002/grl.50200Ashok, K., Behera, S. K., Rao, S. A., Weng, H., & Yamagata, T. (2007). El Niño Modoki and its possible teleconnection. *Journal of Geophysical Research*, *112*(C11), C11007. https://doi.org/10.1029/2006JC003798Bond, N. A., Cronin, M. F., Freeland, H., & Mantua, N. (2015). Causes and impacts of the 2014 warm anomaly in the NE Pacific. *Geophysical Research Letters*, *42*(9), 3414–3420. https://doi.org/10.1002/2015GL063306Capotondi, A., Wittenberg, A. T., Newman, M., Di Lorenzo, E., Yu, J.-Y., Braconnot, P., et al. (2015). Understanding ENSO Diversity. *Bulletin of the American Meteorological Society*, *96*(6), 921–938. https://doi.org/10.1175/BAMS-D-13-00117.1Chang, P., Zhang, L., Saravanan, R., Vimont, D. J., Chiang, J. C. H., Ji, L., et al. (2007). Pacific meridional mode and El Niño-Southern Oscillation. *Geophysical Research Letters*, *34*(16), 1–5. https://doi.org/10.1029/2007GL030302Chiang, J. C. H., & Vimont, D. J. (2004). Analogous Pacific and Atlantic Meridional Modes of Tropical Atmosphere–Ocean Variability. *Journal of Climate*, *17*(21), 4143–4158. https://doi.org/10.1175/JCLI4953.1Chu, P.-S. (1995). Hawaii Rainfall Anomalies and El Niño. *Journal of Climate*, *8*(6), 1697–1703. https://doi.org/10.1175/1520-0442(1995)008<1697:HRAAEN>2.0.CO;2Chu, P.-S., & Chen, H. (2005). Interannual and Interdecadal Rainfall Variations in the Hawaiian Islands*. *Journal of Climate*, *18*(22), 4796–4813. https://doi.org/10.1175/JCLI3578.1Dee, D. P., Uppala, S. M., Simmons, A. J., Berrisford, P., Poli, P., Kobayashi, S., et al. (2011). The ERA-Interim reanalysis: configuration and performance of the data assimilation system. *Quarterly Journal of the Royal Meteorological Society*, *137*(656), 553–597. https://doi.org/10.1002/qj.828Di Lorenzo, E., Schneider, N., Cobb, K. M., Franks, P. J. S., Chhak, K., Miller, A. J., et al. (2008). North Pacific Gyre Oscillation links ocean climate and ecosystem change. *Geophysical Research Letters*, *35*(8), L08607. https://doi.org/10.1029/2007GL032838Di Lorenzo, E., Cobb, K. M., Furtado, J. C., Schneider, N., Anderson, B. T., Bracco, A., et al. (2010). Central Pacific El Niño and decadal climate change in the North Pacific Ocean. *Nature Geoscience*, *3*(11), 762–765. https://doi.org/10.1038/ngeo984Di Lorenzo, E., Liguori, G., Schneider, N., Furtado, J. C., Anderson, B. T., & Alexander, M. A. (2015). ENSO and meridional modes: A null hypothesis for Pacific climate variability. *Geophysical Research Letters*, *42*(21), 9440–9448. https://doi.org/10.1002/2015GL066281Fukumori, I., Wang, O., Fenty, I., Forget, G., Heimbach, P., & Ponte, R. M. (2019). *ECCO Version 4 Release 4*. *Dspace.Mit.Edu* (Vol. 2). Retrieved from https://dspace.mit.edu/handle/1721.1/110380%0Ahttp://hdl.handle.net/1721.1/110380Furtado, J. C., Di Lorenzo, E., Anderson, B. T., & Schneider, N. (2012). Linkages between the North Pacific Oscillation and central tropical Pa-

cific SSTs at low frequencies. *Climate Dynamics*, *39*(12), 2833–2846. https://doi.org/10.1007/s00382-011-1245-4Graham, N. E., & Barnett, T. P. (1987). Sea Surface Temperature , Surface Wind Divergence , and Convection over Tropical Oceans Author (s): N . E . Graham and T . P . Barnett Published by : American Association for the Advancement of Science Stable URL : http://www.jstor.org/stable/1700483 RE. *Science*, *238*(4827), 657–659.Hersbach, H., Bell, B., Berrisford, P., Hirahara, S., Horányi, A., Muñoz-Sabater, J., et al. (2020). The ERA5 global reanalysis. *Quarterly Journal of the Royal Meteorological Society*, (March), qj.3803. https://doi.org/10.1002/qj.3803Jackett, D. R., McDougall, T. J., Feistel, R., Wright, D. G., & Griffies, S. M. (2006). Algorithms for Density, Potential Temperature, Conservative Temperature, and the Freezing Temperature of Seawater. *Journal of Atmospheric and Oceanic Technology*, *23*(12), 1709–1728. https://doi.org/10.1175/JTECH1946.1Johnson, N. C., & Xie, S.-P. (2010). Changes in the sea surface temperature threshold for tropical convection. *Nature Geoscience*, *3*(12), 842–845. https://doi.org/10.1038/ngeo1008Kao, H.-Y., & Yu, J.-Y. (2009). Contrasting Eastern-Pacific and Central-Pacific Types of ENSO. *Journal of Climate*, *22*(3), 615–632. https://doi.org/10.1175/2008JCLI2309.1Kato, S., Rose, F. G., Rutan, D. A., Thorsen, T. J., Loeb, N. G., Doelling, D. R., et al. (2018). Surface Irradiances of Edition 4.0 Clouds and the Earth's Radiant Energy System (CERES) Energy Balanced and Filled (EBAF) Data Product. *Journal of Climate*, *31*(11), 4501–4527. https://doi.org/10.1175/JCLI-D-17-0523.1Kug, J.-S., Jin, F.-F., & An, S.-I. (2009). Two Types of El Niño Events: Cold Tongue El Niño and Warm Pool El Niño. *Journal of Climate*, *22*(6), 1499–1515. https://doi.org/10.1175/2008JCLI2624.1Kutzbach, J. E. (1970). LARGE-SCALE FEATURES OF MONTHLY MEAN NORTHERN HEMISPHERE ANOMALY MAPS OF SEA-LEVEL PRESSURE. *Monthly Weather Review*, *98*(9), 708–716. https://doi.org/10.1175/1520-0493(1970)098<0708:LSFOMM>2.3.CO;2Larson, S. M., Vimont, D. J., Clement, A. C., & Kirtman, B. P. (2018). How Momentum Coupling Affects SST Variance and Large-Scale Pacific Climate Variability in CESM. *Journal of Climate*, *31*(7), 2927–2944. https://doi.org/10.1175/JCLI-D-17-0645.1Lee, T., Fukumori, I., & Tang, B. (2004). Temperature Advection: Internal versus External Processes. *Journal of Physical Oceanography*, *34*(8), 1936–1944. https://doi.org/10.1175/1520-0485(2004)034<1936:TAIVEP>2.0.CO;2Lim, Y., Cullather, R. I., Nowicki, S. M. J., & Kim, K. (2019). Inter-relationship between subtropical Pacific sea surface temperature, Arctic sea ice concentration, and North Atlantic Oscillation in recent summers. *Scientific Reports*, *9*(1), 3481. https://doi.org/10.1038/s41598-019-39896-7Linkin, M. E., & Nigam, S. (2008). The North Pacific Oscillation–West Pacific Teleconnection Pattern: Mature-Phase Structure and Winter Impacts. *Journal of Climate*, *21*(9), 1979–1997. https://doi.org/10.1175/2007JCLI2048.1Luo, X., Wang, B., Frazier, A. G., & Giambelluca, T. W. (2020). Distinguishing Variability Regimes of Hawaiian Summer Rainfall: Quasi-Biennial and Interdecadal Oscillations. *Geophysical Research Letters*, *47*(23).

https://doi.org/10.1029/2020GL091260Moisan, J. R., & Niiler, P. P. (1998). The Seasonal Heat Budget of the North Pacific: Net Heat Flux and Heat Storage Rates (1950–1990). *Journal of Physical Oceanography*, *28*(3), 401–421. https://doi.org/10.1175/1520-0485(1998)028<0401:TSHBOT>2.0.CO;2Ren, H.-L., & Jin, F.-F. (2011). Niño indices for two types of ENSO. *Geophysical Research Letters*, *38*(4), n/a-n/a. https://doi.org/10.1029/2010GL046031Rogers, J. C. (1981). The North Pacific Oscillation. *Journal of Climatology*, *1*(1), 39–57. https://doi.org/10.1002/joc.3370010106Ropelewski, C. F., & Halpert, M. S. (1987). Global and Regional Scale Precipitation Patterns Associated with the El Niño/Southern Oscillation. *Monthly Weather Review*, *115*(8), 1606–1626. https://doi.org/10.1175/1520-0493(1987)115<1606:GARSPP>2.0.CO;2Saha, S., Moorthi, S., Wu, X., Wang, J., Nadiga, S., Tripp, P., et al. (2014). The NCEP Climate Forecast System Version 2. *Journal of Climate*, *27*(6), 2185–2208. https://doi.org/10.1175/JCLI-D-12-00823.1Sanchez, S. C., Amaya, D. J., Miller, A. J., Xie, S.-P., & Charles, C. D. (2019). The Pacific Meridional Mode over the last millennium. *Climate Dynamics*, *53*(5–6), 3547–3560. https://doi.org/10.1007/s00382-019-04740-1Scannell, H. A., Johnson, G. C., Thompson, L., Lyman, J. M., & Riser, S. C. (2020). Subsurface Evolution and Persistence of Marine Heatwaves in the Northeast Pacific. *Geophysical Research Letters*, *47*(23), 1–10. https://doi.org/10.1029/2020GL090548Soares, S. M., Richards, K. J., Bryan, F. O., & Yoneyama, K. (2019). On the Seasonal Cycle of the Tropical South Indian Ocean. Part I: Mixed Layer Heat and Salt Budgets. *Journal of Climate*, *32*(6), 1951–1972. https://doi.org/10.1175/JCLI-D-18-0036.1Stuecker, M. F. (2018). Revisiting the Pacific Meridional Mode. *Scientific Reports*, *8*(1), 3216. https://doi.org/10.1038/s41598-018-21537-0Su, J., Zhang, R., Rong, X., Min, Q., & Zhu, C. (2018). Sea Surface Temperature in the Subtropical Pacific Boosted the 2015 El Niño and Hindered the 2016 La Niña. *Journal of Climate*, *31*(2), 877–893. https://doi.org/10.1175/JCLI-D-17-0379.1Sud, Y. C., Walker, G. K., & Lau, K. M. (1999). Mechanisms regulating sea-surface temperatures and deep convection in the tropics. *Geophysical Research Letters*, *26*(8), 1019–1022. https://doi.org/10.1029/1999GL900197Taylor, G. E. (1984). Hawaiian Winter Rainfall and its Relation to the Southern Oscillation. *Monthly Weather Review*, *112*(8), 1613–1619. https://doi.org/10.1175/1520-0493(1984)112<1613:HWRAIR>2.0.CO;2Tomita, H., Hihara, T., Kako, S., Kubota, M., & Kutsuwada, K. (2019). An introduction to J-OFURO3, a third-generation Japanese ocean flux data set using remote-sensing observations. *Journal of Oceanography*, *75*(2), 171–194. https://doi.org/10.1007/s10872-018-0493-xVimont, D. J., & Kossin, J. P. (2007). The Atlantic Meridional Mode and hurricane activity. *Geophysical Research Letters*, *34*(7), L07709. https://doi.org/10.1029/2007GL029683Vimont, D. J., Battisti, D. S., & Hirst, A. C. (2001). Footprinting: A seasonal connection between the tropics and mid-latitudes. *Geophysical Research Letters*, *28*(20), 3923–3926. https://doi.org/10.1029/2001GL013435Vimont, D. J., Wallace, J. M., & Battisti, D. S. (2003). The Seasonal Footprinting Mechanism in the Pacific: Implications for ENSO. *Journal of Climate*, *16*(16), 2668–2675. https://doi.org/10.1175/1520-0442(2003)016<2668:TSFMIT>2.0.CO;2Yu,

J.-Y., Kao, P., Paek, H., Hsu, H.-H., Hung, C., Lu, M.-M., & An, S.-I. (2015). Linking Emergence of the Central Pacific El Niño to the Atlantic Multidecadal Oscillation. *Journal of Climate*, *28*(2), 651–662. https://doi.org/10.1175/JCLI-D-14-00347.1Yu, L., Jin Xiangze, & Weller, A. R. (2008). *Multidecade Global Flux Datasets from the Objectively Analyzed Air-sea Fluxes (OAFlux) Project: Latent and Sensible Heat Fluxes, Ocean Evaporation, and Related Surface Meteorological Variables. Woods Hole Oceanographic Institution OAFlux Project Technical Report (OA-2008-01).* https://doi.org/10.1007/s00382-011-1115-0Zhang, C. (1993). Large-Scale Variability of Atmospheric Deep Convection in Relation to Sea Surface Temperature in the Tropics. *Journal of Climate*, *6*(10), 1898–1913. https://doi.org/10.1175/1520-0442(1993)006<1898:LSVOAD>2.0.CO;2Zhu, Z., & Li, T. (2017). The Record-Breaking Hot Summer in 2015 over Hawaii and Its Physical Causes. *Journal of Climate*, *30*(11), 4253–4266. https://doi.org/10.1175/JCLI-D-16-0438.1 Zuo, H., Balmaseda, M.A., Mogensen, K. and Tietsche, S. (2018). OCEAN5: The ECMWF Ocean Reanalysis System and its real-time analysis component. Technical Report 823, ECMWF, Reading, UK.